RSC Advances

ROYAL SOCIETY OF CHEMISTRY

www.rsc.org/advances

RSC Advances

ARTICLE

In-situ growth of urchin-like $NiCo_2S_4$ hexagonal pyramid microstructures on 3D graphene nickel foam for enhanced performance of supercapacitors

Received 00th January 20xx,
Accepted 00th January 20xx

DOI: 10.1039/x0xx00000x

www.rsc.org/

Xiaoli Wang[a,b], Xianjun Xia[a], Lemu Girma Beka[b], Weihua Liu[b], Xin Li[b*]

Urchin-like $NiCo_2S_4$ hexagonal pyramid microstructures have been in-situ grown on three dimensional (3D) graphene nickel foam (GNF) by two-step hydrothermal method, labeled as NCS-GNF. The presence of graphene between nickel cobalt sulphur (NCS) and nickel foam (NF) can effectively improve ion and charge transportation. As a binder-free electrode for supercapacitors, it exhibits an ultrahigh specific capacitance of 9.6 F cm^{-2} at 10 mA cm^{-2} with excellent rate performance and cycling stability at a mass loading of 5.8 mg cm^{-2} , corresponding to a mass specific capacitance of about 1650 F g^{-1} at 1.7 A g^{-1}. The excellent electrochemical performance of urchin-like NCS-GNF is attributed to its unique microstructure. This unique microstructure electrode material has a promising application for capacitors in future.

Introduction

Due to their higher power density, long cycling lifespan, short charging time, and low maintenance cost, electrochemical capacitors have attracted considerable attention in recent years[1-3]. Because of their significant advantages, they have quickly become the potential choice for energy storage.

Generally, the performance of supercapacitor is determined by properties of the electrode materials and its electrode fabrication processing. Up to now, a large amount of active materials (carbon-based materials, conducting polymers and transition metal compounds) have been well studied. Unfortunately, they all have shown their disadvantages for application, such as the low specific capacitance in carbon based materials, the low conductivity in transition metal oxides, and the poor cycling stability in conducting polymers[4-7]. In recent years, $NiCo_2S_4$ has shown excellent electrochemical performance, due to its higher electrochemical activity and higher capacity than mono-metal sulphides based on richer redox reactions[8, 9]. It has been reported that $NiCo_2S_4$ porous nanotubes and urchin-like nanostructures were used as supercapacitor electrode materials and have shown good electrochemical activities of 933 F g^{-1} at 1 A g^{-1} and 1149 F g^{-1} at 1 A g^{-1}, respectively[10, 11]. Lou et al. fabricated $NiCo_2S_4$ hollow nanoprisms with a high capacitance of 895 F g^{-1} at 1 A g^{-1} and excellent cycling stability[12]. However, in all these reports they fabricated the electrode by coating of the active material on current collector by using polymer binder which seriously affect the electrochemical performance of the capacitors by increasing dead mass and limiting the conductivity of the electrode[8, 13].

3D graphene foam was firstly fabricated by using a nickel foam as a substrate via chemical vapor deposition (CVD) by Cheng et al[14]. It is a well-designed graphene network with high conductivity and high specific surface area, which can promote the penetration of electrolyte and the transportation of ions, and significantly enhance the electrochemical performance, and has been applied in many fields, especially served as the scaffold for composite electrodes[13, 15, 16]. Mei Yu et al. fabricated a nano-sized needle-shape structure of $NiCo_2O_4$ on GNF with a high specific capacitance of 1588 F g^{-1} at 1 A g^{-1} [12]. As a new trend for the development of supercapacitors, researchers are making their best effort to fabricate electrode without polymer binder to improve electrochemical behavior.

Synthesizing the above considerations, in our work, urchin-like $NiCo_2S_4$ were grown on 3D graphene nickel foam (GNF) through a three-step method. Firstly, graphene was grown on pure nickel foam (NF) by CVD method. Then, urchin-like $NiCo_2S_4$ was synthesized on GNF via two-step hydrothermal treatment. As a binder-free electrode, we expect to get good electrochemical performance of high specific capacitance and rate capability along with good cycling stability.

[a] School of Science.
[b] School of Electronics and Information Engineering.
Xi'an Jiaotong University, Xi'an, Shaanxi, China, 710049
E-mail: * lx@xjtu.edu.cn

Experimental

Fabrication of urchin-like $NiCo_2S_4$ microstructures on GNF

As shown in figure 1, urchin-like $NiCo_2S_4$ on GNF (NCS-GNF) was prepared by three steps.

Step Ⅰ: 3D GNF was made via CVD method to be used as a substrate for depositing active material[14, 17]. Firstly, the NF (4cm×2cm) was treated respectively with acetone and ethanol for 10 minutes to remove the surface impurity, and washed ultrasonically with deionized (DI) water and dried. Secondly, NF was put into the quartz tube of CVD furnace and heated to 1023 ℃ in 80 minutes, maintained at 1023℃ for 20 minutes under argon (100sccm) gas atmosphere. Then H_2 (100sccm) and CH_4 (2sccm) gas were flew into the quartz tube for 90 minutes to grow graphene layer on NF. Finally, the sample was cooled down rapidly to room temperature with the gas protection of H_2. Step Ⅱ: Before the synthesis of $NiCo_2S_4$, the loading of the precursor was done by hydrothermal treatment. In a typical procedure, 4 mmol $NiCl_2.6H_2O$, 8 mmol $CoCl_2.6H_2O$ and 20 mmol urea were added to get 60 mL deionized water solution and stirred for 15 minutes. The claret-red solution was transferred into an 80 mL Teflon-lined stainless-steel autoclave. Then a piece of pre-prepared GNF was put into the autoclave. The autoclave was sealed and maintained at 120℃ for 6 h. After cooling down naturally to the room temperature, the GNF with precursor was taken out and washed by ethanol and DI water with several times for the future work. Step III: To get $NiCo_2S_4$, Na_2S was employed to transfer the precursor into sulphide deposit. 5 mmol Na_2S was added in deionized water by stirring for 15 minutes to get 60 mL transparent solution. Then the solution and the nickel cobalt precursor on GNF was transferred into a 80 mL Teflon-lined stainless-steel autoclave, which also was sealed and maintained at 120℃for 6 h. When the temperature restored up to room temperature, the final product was taken out, washed by DI water for 4 times and dried at 60℃ for 4 h.

Materials Characterization

Scanning electron microscopy (SEM) and element mapping images were taken by Hitachi S-4800 microscope to check the morphology and elemental distribution of our samples respectively. To obtain the data of the crystal structure of NCS, XRD patterns were recorded on a Rigaku Max-2200 X-ray diffractometer with monochromatized Cu_{Ka} radiation (λ=0.1542 nm). Raman spectroscopy was carried out by HR800 with an excitation wavelength of 633 nm.

Electrochemical measurements

The electrochemical performance was measured in a three electrode system with an Ag/AgCl saturated KCl reference electrode and a Pt counter electrode in 6 M KOH solution[18]. NF or GNF with urchin-like $NiCo_2S_4$ microstructures was cut into 1cm×1cm quadrate shape and acted directly as the working electrode. The mass loading of $NiCo_2S_4$ on GNF electrode (1cm×1cm) is about 5.8 mg. To examine the supercapacitive performance, cyclic voltammetry (CV), galvanostatic charge-discharge (GCD) and electrochemical impedance spectroscopy (EIS) method were employed.

The specific capacitance (*C*) of the electrode can be calculated according to the following equation[19, 20]:

$$C_m = \frac{I \times \Delta t}{m \times \Delta V} \qquad (1)$$

C_m [$F\ g^{-1}$] is the specific capacitance of the electrode based on the mass of active materials, I [A] is the discharge current, m [g] is the loading mass of active material, ΔV [V] is the charge-discharge window. Sometimes, we use area specific capacitance C_s [$F\ cm^{-2}$], we only need to change the m of equation to S [cm^2], where S is the effective area of electrode[21].

$$C_s = \frac{I \times \Delta t}{S \times \Delta V} \qquad (2)$$

Results and Discussion

Material Characterization

GNF was characterized by SEM, energy-dispersive X-ray spectroscopy (EDS) and Raman. Figure 2 (a) and (b) are the SEM images of GNF, from which we can recognize a thin film on NF. In figure 2 (b), we can clearly see the white texture, as the label with arrows, which may be caused by the film partially exfoliated from the substrate, because NF is not flat[22]. The pore size of 3D GNF network is about 200 μm, which has advantages in improving electron conductivity and the contact between electrolyte and electrode material[13]. Figure 2 (c), Raman spectra of GNF, clearly demonstrates the two characteristics carbon bonding bands, G band around 1580 cm^{-1} and 2D band around 2700 cm^{-1}. The intensity ratio of I_{2D}/I_G and shape of 2D band are sensitive to the number of graphene layers. The I_{2D}/I_G ratio in figure 2 (d) is about 2.5:1, which can prove that the film on NF is few-layer (less than 5 layers) graphene[22-24]. Figure 2 (d) shows the typical low resolution SEM image of NCS-GNF. Apparently, the NCS is uniformly covered on the 3D GNF and maintaining the original grid structure. Figure 2 (e) shows the representative SEM image of the sample. Obviously, the NCS displays a kind of uniform urchin-like structures and a large amount of urchin-like clusters are stacked together. In figure 2 (f), the cross-section SEM image of NCS is regular hexagon and the distance between the two opposite sides of hexagon is about 500 nm, which demonstrates that the active material maintains hexagonal pyramid microstructures.

As shown in figure 3 (a-e), scanning electron microscopic elemental mapping was employed on GNF and NCS-GNF to measure the elemental distribution. Figure 3 (a) displays the elemental mapping of carbon on NF. The mapping image of carbon on NF shows uniform and continuous dispersion, which suggests that graphene was covered over all the NF. From figure 3 (b), the uniform and continuous coverage of carbon, which seems to be more light-colored than image (a), suggests that graphene is continuously coated on NF after the whole process of getting NCS-GNF electrode. The elemental mapping images of sulphur,

cobalt and nickel in image (c), (d) and (e) exhibit the homogeneous growth of NCS on GNF. Figure 3 (f) shows the XRD pattern of NCS-GNF. From the image, two strong diffraction peaks at 2 theta=44.7^0, 52.1^0 correspond to (111), (200) planes of nickel foam respectively. The weak diffraction peak around 21.9^0 is indexed into (002) planes of graphene[25-27]. Except for the above diffraction peaks, all the other diffraction peaks are in accordance with the cubic type $NiCo_2S_4$ (JCPDS Card no. 43-1477), indicating successful fabrication of $NiCo_2S_4$ on GNF.

Characterization of Electrochemical Performances

The supercapacitive performance of NCS-GNF electrode was respectively tested by CV, GCD and EIS techniques on a CS 2350 (Corrtest, Wuhan, China) electrochemical workstation. In comparative experiment, the GNF and NCS-NF were measured to study the difference and improvement of electrochemical properties after the introduction of graphene.

Figure 4 (a) is the CV curves of GNF and NCS-GNF at a scan rate of 10 mV s^{-1}. Obviously, the CV integrated area of NCS-GNF are much larger than the area of GNF, which indicates that the active material on GNF play a leading role in electrochemical performance and we can ignore the influence of substrate to capacitance. Figure 4 (b) is the typical CV curves of NCS-GNF with the potential window from -0.2 to 0.6 V (VS Ag/AgCl reference electrode) at various scan rates ranging from 1 to 20 mV s^{-1}. Clearly, two pairs of redox peaks in each curve, particularly at low scan rates, suggest that the pseudo capacitive behavior of NCS, apparently different from the EDLCs characterized by nearly rectangular CV curves[7, 27]. With a 20-fold increment in the sweep rate, from 1 to 20 mV s^{-1}, there were no significant changes in the shape and position, indicating that NCS-GNF electrode is suitable for fast redox reactions. The obvious redox peaks in all CV can be attributed to the redox reactions, based on the following equations[28, 29]:

$$NiCo_2S_4 + 2OH^- = NiS_{4-2x}OH + 2CoS_xOH + 2e^- \quad (3)$$

$$CoS_x + OH^- = CoS_xO + H_2O + e^- \quad (4)$$

Figure 5 (a) shows the GCD properties of GNF and NCS-GNF at a current density of 10 mA cm^{-2}. Compared with NCS-GNF, the discharge time of GNF is almost negligible, which can also highlight the leading role of NCS in electrochemical performance. Figure 5 (b) and (c) present the GCD curves of NCS-GNF electrode with a potential window of -0.1 to 0.49 V (VS Ag/AgCl reference electrode) at various current densities ranging from 10 mA cm^{-2} to 100 mA cm^{-2}. The apparent flat regions match very well with the redox peaks of CV curves, which indicate the existence of faradaic pseudo capacitance. Moreover, the symmetrical properties of GCD curves at various current densities imply the excellent electrochemical reversibility and charge-discharge properties of the electrode. The multiple plateaus of every charge-discharge curve suggest the multi-step redox reaction, caused by the coexistence of the nickel ions and cobalt ions[1]. The specific capacitance can be calculated according to the GCD curves by equation (2) and plotted in Figure 5 (d), which shows that the specific capacitance of the electrode gradually decreases with the increase of current density and still keeps a high value of 7.6 F cm^{-2} at 100 mA cm^{-2}. At the current density of 10 mA cm^{-2} , NCS-GNF electrode shows a specific capacitance of 9.6 F cm^{-2} , corresponding to a mass specific capacitance of about 1650 F g^{-1}, much higher than 1149 F g^{-1} at 1 A g^{-1} of Chen et al[11]. About 79.1% of the capacitance for NCS-GNF is retained when the current density increases from 10 to 100 mA cm^{-2}, which may be caused by the introduction of graphene and in-situ process.

In figure 6 (a) and (b), NCS-NF and NCS-GNF were compared in CV and GCD, respectively. From figure 6 (a), it's obvious that the CV integrated area of NCS-GNF is much larger than that of NCS-NF. In figure 6 (b), NCS-GNF electrode exhibits a wider GCD window and longer discharge time than NCS-NF electrode at 13.8 A g^{-1}. Both (a) and (b) can fully indicate that NCS-GNF electrode exhibits much better electrochemical performance than NCS-NF. Figure 6 (c) demonstrates that NCS-GNF electrode shows significantly higher specific capacitance and better stability than NCS-NF electrode when the charge-discharge current densities increase. All the enhanced performance maybe be attributed to the facts that the highly conductive graphene coating between NCS and NF ensures rapid charge transfer from NCS to NF.

Figure7 (a) shows a plot of the specific capacitance as a function of cycle number at a current density of 13.8 A g^{-1}. The NCS-GNF electrode exhibits excellent cycling stability of nearly 100% after 3000 times of charge discharge. Because of the relatively good electrical conductivity of $NiCo_2S_4$, both NCS-GNF and NCS-NF have exhibited good cycling stability. However, NCS-GNF electrode always has a larger mass specific capacitance than NCS-NF electrode, which may be attributed to the excellent mechanical contact of NiCo2S4 to GNF.

To further understand the electrochemical characteristic of electrode material, EIS was employed on NCS-GNF and NCS-NF electrode. Figure 7 (b) describes the impedance responses of NCS-GNF and NCS-NF electrode, which were measured at the open-circuit potential in the frequency ranging from 100 KHz to 0.01 Hz with an AC amplitude of 5 mV. In the Nyquist plots, high frequency semicircle corresponds to the charge transfer resistance and low frequency curve is related to capacitance behavior[30]. From the inset image of figure5 (b), the intercept with the real axis (R_s) and diameter of semicircle (R_{ct}) of NCS-GNF electrode (R_s=0.5Ω, R_{ct}=0.25Ω) are smaller than those of NCS-NF electrode, indicating lower diffusion resistance and higher charge-transfer rate between the electrolyte and the active material because of the introduction of graphene.

In a word, NCS-GNF electrode has shown excellent electrochemical properties. In terms of its good performance, we suppose that it can be attributed to several reasons: (1) 3D GNF acts as a perfect current collector with a lot of porous and excellent electronic transport capacity, which provides high pathways for the transfer of ions and electrons[31]. Lower charge transfer resistance of NCS-GNF than that of NCS-NF makes charge transfer from electrolyte to NF more quickly. (2) Unique urchin-like $NiCo_2S_4$ hexagonal pyramid microstructures possess a large contact area with the electrolyte, which is good for its performance[11]. (3) The in-situ growth process also leads to efficient utilization of active materials by avoid using polymer binder, which adds the dead mass and extra contact resistance of active material. (4) The inherent characteristics of $NiCo_2S_4$, richer redox activity and good conductivity[8, 9, 32], make it become a promising material for supercapacitor.

Conclusions

In summary, the urchin-like $NiCo_2S_4$ hexagonal pyramid microstructures on 3D graphene nickel foam have been successfully prepared and shown excellent electrochemical performance in supercapacitor. The in-situ NCS-GNF electrode exhibits an ultrahigh specific capacitance of 9.6 F cm^{-2} at the discharge rate of 10 mA cm^{-2} with a high $NiCo_2S_4$ mass loading of about 5.8 mg cm^{-2} on GNF, being equivalent to 1650 F g^{-1} at 1.7 A g^{-1}. It also has shown good cycling stability and good rate capability. The outstanding electrochemical performance of NCS-GNF is mainly attributed to the well design of 3D GNF combined with urchin-like $NiCo_2S_4$ hexagonal pyramid microstructures and the introduction of graphene, providing large contact area and high transport pathways for ions and electrons.

Acknowledgements

This work was financially supported by grants from the National Natural Science Foundation of China (No. 91123018, 61172040, 61172041), Shaanxi Natural Science Foundation (2014JM7277), and the Fundamental Research Funds for the Central Universities. Some SEM work was done at International Center for Dielectric Research (ICDR), Xi'an Jiaotong University, Xi'an, China; Authors also thank Ms. Dai and Mr. Yang for their help in using SEM.

Notes and references

1. H. Chen, J. Jiang, L. Zhang, D. Xia, Y. Zhao, D. Guo, T. Qi and H. Wan, *Journal of Power Sources*, 2014, **254**, 249-257.
2. M. Zhi, C. Xiang, J. Li, M. Li and N. Wu, *Nanoscale*, 2013, **5**, 72-88.
3. P. Simon and Y. Gogotsi, *Nature materials*, 2008, **7**, 845-854.
4. D. N. Futaba, K. Hata, T. Yamada, T. Hiraoka, Y. Hayamizu, Y. Kakudate, O. Tanaike, H. Hatori, M. Yumura and S. Iijima, *Nature materials*, 2006, **5**, 987-994.
5. C. Yuan, H. B. Wu, Y. Xie and X. W. D. Lou, *Angewandte Chemie International Edition*, 2014, **53**, 1488-1504.
6. G. A. Snook, P. Kao and A. S. Best, *Journal of Power Sources*, 2011, **196**, 1-12.
7. W. Hu, R. Chen, W. Xie, L. Zou, N. Qin and D. Bao, *ACS applied materials & interfaces*, 2014, **6**, 19318-19326.
8. J. Pu, T. Wang, H. Wang, Y. Tong, C. Lu, W. Kong and Z. Wang, *ChemPlusChem*, 2014, **79**, 577-583.
9. L. Shen, J. Wang, G. Xu, H. Li, H. Dou and X. Zhang, *Advanced Energy Materials*, 2015, **5**.
10. H. Wan, J. Jiang, J. Yu, K. Xu, L. Miao, L. Zhang, H. Chen and Y. Ruan, *CrystEngComm*, 2013, **15**, 7649-7651.
11. H. Chen, J. Jiang, L. Zhang, H. Wan, T. Qi and D. Xia, *Nanoscale*, 2013, **5**, 8879-8883.
12. X.-W. Wang, X.-Z. Li, K.-L. Wu, M.-L. Zhao, Y.-X. Yue, J. Cheng, C.-C. Ma, J. Ming and X.-W. Wei, *Chemistry Letters*, 2014, **43**, 1590-1592.
13. M. Yu, J. Chen, J. Liu, S. Li, Y. Ma, J. Zhang and J. An, *Electrochimica Acta*, 2015, **151**, 99-108.
14. Z. Chen, W. Ren, L. Gao, B. Liu, S. Pei and H.-M. Cheng, *Nature materials*, 2011, **10**, 424-428.
15. B. Zhan, C. Liu, H. Chen, H. Shi, L. Wang, P. Chen, W. Huang and X. Dong, *Nanoscale*, 2014, **6**, 7424-7429.
16. X. Dong, Y. Cao, J. Wang, M. B. Chan-Park, L. Wang, W. Huang and P. Chen, *RSC Advances*, 2012, **2**, 4364-4369.
17. X. Cao, Y. Shi, W. Shi, G. Lu, X. Huang, Q. Yan, Q. Zhang and H. Zhang, *Small*, 2011, **7**, 3163-3168.
18. H. Wang, X. Sun, Z. Liu and Z. Lei, *Nanoscale*, 2014, **6**, 6577-6584.
19. Q. Wang, J. Xu, X. Wang, B. Liu, X. Hou, G. Yu, P. Wang, D. Chen and G. Shen, *ChemElectroChem*, 2014, **1**, 559-564.
20. G. Q. Zhang, H. B. Wu, H. E. Hoster, M. B. Chan-Park and X. W. D. Lou, *Energy & Environmental Science*, 2012, **5**, 9453-9456.
21. L. Huang, D. Chen, Y. Ding, S. Feng, Z. L. Wang and M. Liu, *Nano letters*, 2013, **13**, 3135-3139.
22. A. Obraztsov, E. Obraztsova, A. Tyurnina and A. Zolotukhin, *Carbon*, 2007, **45**, 2017-2021.
23. Z. H. Ni, T. Yu, Y. H. Lu, Y. Y. Wang, Y. P. Feng and Z. X. Shen, *ACS nano*, 2008, **2**, 2301-2305.
24. A. Malesevic, R. Vitchev, K. Schouteden, A. Volodin, L. Zhang, G. Van Tendeloo, A. Vanhulsel and C. Van Haesendonck, *Nanotechnology*, 2008, **19**, 305604.
25. A. Ferrari, J. Meyer, V. Scardaci, C. Casiraghi, M. Lazzeri, F. Mauri, S. Piscanec, D. Jiang, K. Novoselov and S. Roth, *Physical review letters*, 2006, **97**, 187401.
26. E. Dervishi, Z. Li, F. Watanabe, A. Biswas, Y. Xu, A. R. Biris, V. Saini and A. S. Biris, *Chem. Commun.*, 2009, 4061-4063.
27. C. Yuan, J. Li, L. Hou, X. Zhang, L. Shen and X. W. D. Lou, *Advanced Functional Materials*, 2012, **22**, 4592-4597.
28. L. Mei, T. Yang, C. Xu, M. Zhang, L. Chen, Q. Li and T. Wang, *Nano Energy*, 2014, **3**, 36-45.
29. L. Shen, L. Yu, H. B. Wu, X.-Y. Yu, X. Zhang and X. W. D. Lou, *Nature communications*, 2015, **6**.
30. J. Ji, L. L. Zhang, H. Ji, Y. Li, X. Zhao, X. Bai, X. Fan, F. Zhang and R. S. Ruoff, *ACS nano*, 2013, **7**, 6237-6243.
31. D. W. Wang, L. Feng, L. Min, G. Q. Lu and H. M. Cheng, *Angewandte Chemie*, 2007, **120**, 379–382.
32. H. Wan, J. Liu, Y. Ruan, L. Lv, L. Peng, X. Ji, L. Miao and J. Jiang, *ACS applied materials & interfaces*, 2015, **7**, 15840-15847.

Figure caption

Figure.1 Schematic illustration for the fabrication of NCS-GNF.

Figure.2 (a) SEM image of GNF; (b) high resolution image of the white elliptical section in (a); (c) Raman spectra of GNF, taken on the skeleton of GNF, as the callout with oval outline in (a); (d) (e) SEM images of NCS-GNF, (e) is the high resolution image of the callout with oval outline in (d); (f) cross-section image of NCS-GNF in the circle part of (e).

Figure.3 (a) EDS elemental mapping image of carbon on GNF; (b-e) EDS elemental mapping images of carbon, sulphur, cobalt and nickel of NCS-GNF; (f) XRD spectra of NCS-GNF.

Figure.4 (a) CV curves of NCS-GNF compared with GNF at a scan rate of 10 mv s^{-1}. (b) CV curves of NCS-GNF with different scan rates.

Figure.5 (a) GCD curves of NCS-GNF compared with GNF at 10 mA cm^{-2}; (b) (c) GCD curves of NCS-GNF at different charge-discharge current density; (d) Specific capacitance as a function of the current density of NCS-GNF.

Figure.6 (a) (b) CV and GCD curves of NCS-GNF electrode compared with NCS-NF electrode at a current density of 10 mA cm^{-2} and 13.8 A g^{-1}, respectively; (c) Mass specific capacitance as a function of the current density of NCS-NF and NCS-GNF.

Figure.7 (a) Cycling performance of the NCS-GNF and NCS-NF at a constant charge-discharge current density of 13.8 A g^{-1} for 3000 times; (b) Nyquist plots of NCS-GNF and NCS-NF at the open-circuit potential.

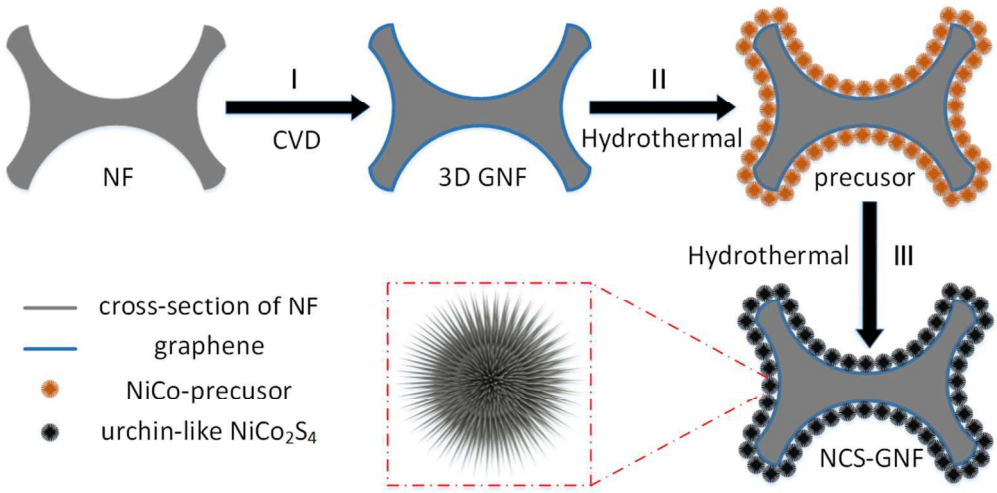

295x146mm (96 x 96 DPI)

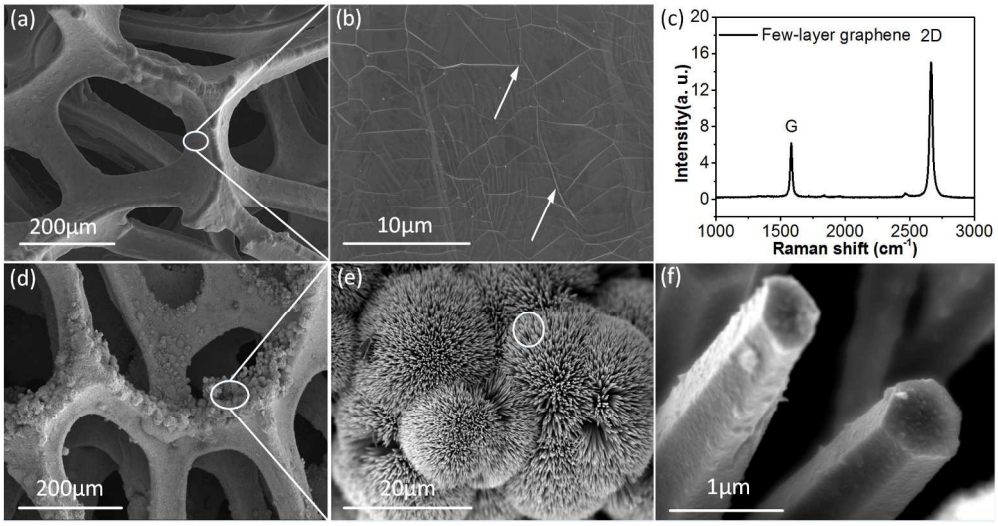

533x280mm (96 x 96 DPI)

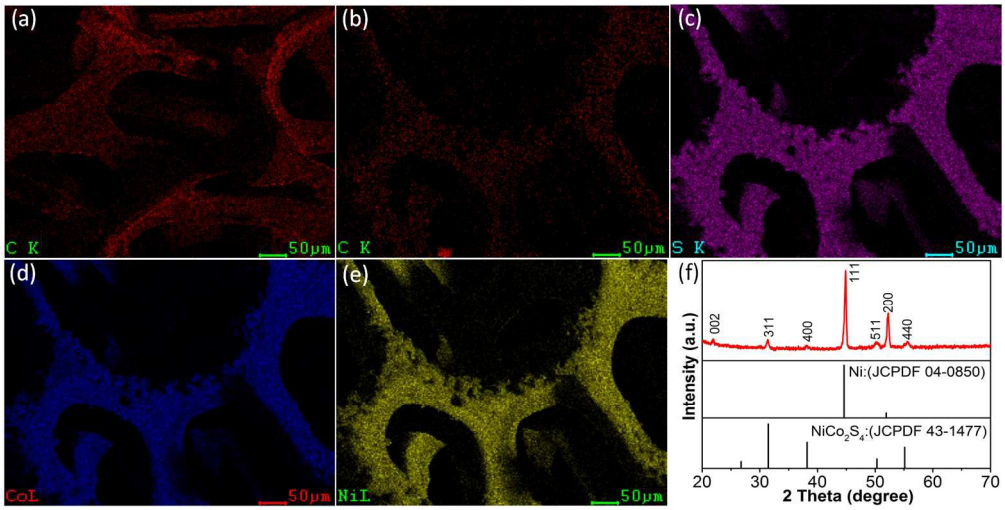

525x263mm (96 x 96 DPI)

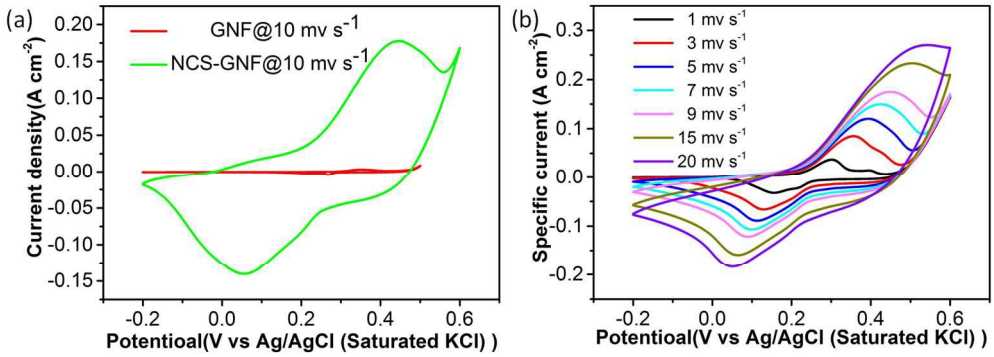

493x175mm (96 x 96 DPI)

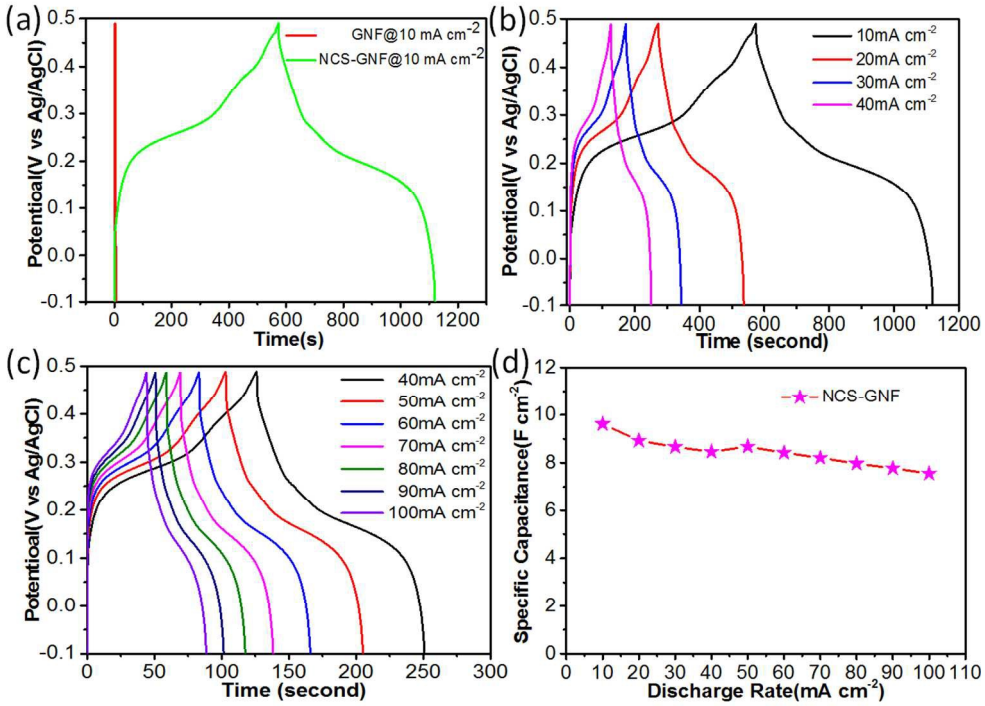

358x257mm (96 x 96 DPI)

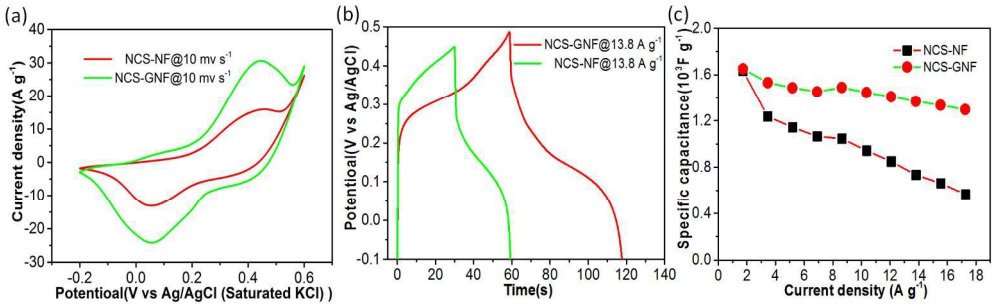

586x180mm (96 x 96 DPI)

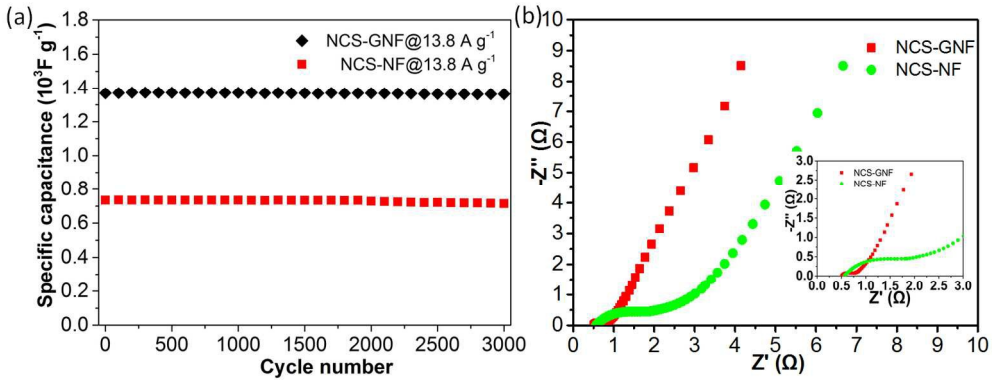

491x190mm (96 x 96 DPI)